INSTITUT DE FRANCE
Académie des sciences

Comptes Rendus

Mécanique

Tsorng-Whay Pan, Shang-Huan Chiu, Aixia Guo and Jiwen He

Numerical study of transitions in lid-driven flows in shallow cavities

Published online: 7 February 2023

https://doi.org/10.5802/crmeca.166

Part of Special Issue: The scientific legacy of Roland Glowinski

Guest editors: Gregoire Allaire (CMAP, Ecole Polytechnique, Institut Polytechnique de Paris, Palaiseau, France), Jean-Michel Coron (Laboratoire Jacques-Louis Lions, Sorbonne Université) and Vivette Girault (Laboratoire Jacques-Louis Lions, Sorbonne Université)

Les Comptes Rendus. Mécanique *sont membres du Centre Mersenne pour l'édition scientifique ouverte*
www.centre-mersenne.org
e-ISSN : 1873-7234

Comptes Rendus
Mécanique
Published online: 7 February 2023
https://doi.org/10.5802/crmeca.166

The scientific legacy of Roland Glowinski / *L'héritage scientifique de Roland Glowinski*

Numerical study of transitions in lid-driven flows in shallow cavities

Tsorng-Whay Pan *, [a], **Shang-Huan Chiu** [b], **Aixia Guo** [a] and **Jiwen He** [a]

[a] Department of Mathematics, University of Houston, Houston, Texas 77204, USA

[b] Department of Mathematics, Lehigh University, Bethlehem, PA, 18015, USA

E-mails: pan@math.uh.edu (T.-W. Pan), schiu.twn@gmail.com (S.-H. Chiu), gax8118@gmail.com (A. Guo), jiwenhe@math.uh.edu (J. He)

In memory of Professor Roland Glowinski

Abstract. In this article, three dimensional (3D) lid-driven flow in shallow cavities with a unit square base are studied. The numerical solution of the Navier–Stokes equations modeling incompressible viscous fluid flow in a cavity is obtained via a methodology combining a first order accurate operator-splitting scheme, a L^2-projection Stokes solver, a wave-like equation treatment of the advection and finite element space approximations. Numerical results of a lid-driven flow in a cubic cavity show a good agreement with those reported in literature. The critical Reynolds numbers (Re_{cr}) for having flow with increasing of oscillating amplitude (a Hopf bifurcation) in different shallow cavities are obtained and associated oscillating modes are studied.

Keywords. Lid driven cavity flow, Shallow cavity, Taylor–Görtler-like vortices, Hopf bifurcation, Projection method.

Published online: 7 February 2023

1. Introduction

Lid-driven cavity flow is a classical flow situation that has attracted much attention due to its flow configuration relevant to many industrial applications, such as coating and melt-spinning processes pointed out in [1], and its importance to the basic study of fluid mechanics, including boundary layers, eddies, secondary flows, complex three-dimensional patterns, various instabilities and transition, chaotic, and turbulent, as discussed in a review paper by Shankar and Deshpande in [2]. Also its geometrical simplicity and unambiguous boundary conditions facilitate experimental calibrations and numerical computations, thus providing an ideal benchmark problem for validating numerical methods and comparing results obtained from laboratory and computational experiments.

It is known that, depending on the solution method, boundary conditions and mesh size used in simulation, the critical Reynolds number (Re_{cr}) for the occurrence of transition from

* Corresponding author.

steady flow to oscillatory flow (a Hopf bifurcation) in two-dimensional square lid-driven cavity flow varies between 8000 and 10,000 (e.g., see [3–7]). The oscillatory instability in cubic lid-driven cavity flows has been studied recently in [8–11]. Numerically, Feldman and Gelfgat [8] obtained that the critical Reynolds number for the occurrence of such Hopf bifurcation is at $Re_{\rm cr} = 1914$. Anupindi *et al.* [10] reported that their critical value is $Re_{\rm cr} = 2300$ (but it was obtained with regularized boundary conditions). Kuhlmann and Albensoeder's critical Reynolds number is at $Re_{\rm cr} = 1919.51$ as obtained in [11]. Experimentally, Liberzon *et al.* [9] reported that the critical Reynolds number is in the range [1700, 1970], which is slightly lower than $Re = 2000$, at which Iwatsu *et al.* [12] obtained a pair of Taylor–Görtler-like (TGL) vortices for a cubic lid-driven cavity flow. Giannetti *et al.* obtained that the cubic lid-driven cavity flow becomes unstable for Re just above 2000 via the three-dimensional global linear stability analysis reported in [13].

In this article, we have studied numerically the transition from steady flow to oscillatory flow in shallow cavities with a unit square base. We have applied a first order accurate operator-splitting scheme (the Lie scheme, [14]) to the numerical solution of the Navier–Stokes equations, which is an extension of the investigations reported in [7, 15, 16]. The resulting methodology is easy to implement and quite modular since, at each time step, one has to solve a sequence of three simpler sub-problems. For the first sub-problem we have used a L^2-projection Stokes solver à la Uzawa to force the incompressibility condition. To solve the advection problem as the second sub-problem, we have applied a wave-like equation method (see, e.g., [17, 18]). The third sub-problem is a diffusion problem which can be solved easily. The numerical results for a lid-driven flow in a cubic cavity show a good agreement with numerical and experimental results available in the literature (see Section 3.1). For investigating the mode associated with the transition from steady flow to oscillatory flow in shallow cavities, we have focused on the flow fields at Re close to $Re_{\rm cr}$. The distortion of flow field with respect to the averaged flow field in one period of the oscillation shows periodic behavior of vortices close to the bottom wall and next to the upstream wall. The change of those oscillating modes in shallow cavities has been studied for different cavity heights. The outline of this article is as follows: We first introduce the formulation of flow problem and then the numerical methods briefly in Section 2. In Section 3, numerical results obtained for lid-driven flow in a cubic cavity are compared with numerical and experimental results available in literature. Then critical Reynolds numbers for the transition from steady flow to oscillatory flow in shallow cavities are obtained and the connection between oscillatory flow and oscillating mode is investigated. Conclusions are summarized in Section 4.

2. Problem formulation

The governing equations for modeling incompressible viscous Newtonian fluid flow in a cavity $\Omega \subset \mathbb{R}^3$ (see Figure 1) for $T > 0$ are the Navier–Stokes equations, namely

$$\frac{\partial \mathbf{u}}{\partial t} - \nu \Delta \mathbf{u} + (\mathbf{u}\cdot\nabla)\mathbf{u} + \nabla p = \mathbf{f} \quad \text{in } \Omega \times (0,T), \tag{1}$$

$$\nabla \cdot \mathbf{u} = 0 \quad \text{in } \Omega \times (0,T), \tag{2}$$

$$\mathbf{u}(0) = \mathbf{u}_0, \quad \text{with } \nabla \cdot \mathbf{u}_0 = 0, \tag{3}$$

$$\mathbf{u} = \mathbf{u}_B(\mathbf{x}) \quad \text{on } \partial\Omega \times (0,T) \text{ with } \int_{\partial\Omega} \mathbf{u}_B \cdot \mathbf{n}\, d\boldsymbol{\gamma} = 0 \text{ on } (0,T), \tag{4}$$

where $\mathbf{u}$ and p are the flow velocity and pressure, respectively, ν is a viscosity coefficient, $\mathbf{f}$ is the body force, $\mathbf{u}_B(\mathbf{x})$ is the boundary data, and $\mathbf{n}$ is the unit outward normal vector at the boundary $\boldsymbol{\gamma} = \partial\Omega$. We denote by $\nu(t)$ the function $\mathbf{x} \to \nu(\mathbf{x}, t)$, $\mathbf{x}$ being the generic point of $\mathbb{R}^3$.

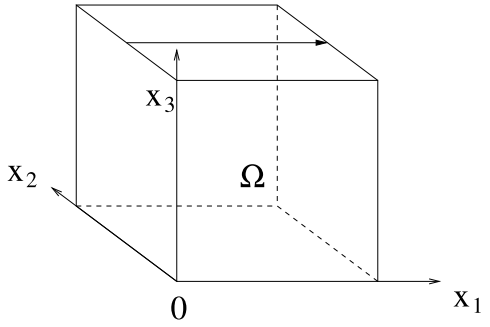

Figure 1. Cubic cavity of edge length 1.

The numerical solution of problem (1)–(4) has generated a most abundant literature. Following Chorin [19, 20] and Temam [21, 22], most "modern" Navier–Stokes solvers are based on operator splitting algorithms (see, e.g., Refs. [23, 24], [25, Chapter 3] and [26, Chapters 2 and 7]) in order to force the incompressibility condition via either H^1-projection or L^2-projection Stokes solver method. Among those methods which can be applied to the numerical solution of (1)–(4), we have chosen one based on the Lie scheme (see, e.g., see [26, 27] for a general discussion of that scheme). It is first order accurate in time, but its low order time accuracy is compensated by its modularity, easy implementation, stability, and robustness properties. To speed up the numerical solution of the cubic lid-driven cavity flow problem, we have time-discretized the related problem (1)–(4), using a three stage Lie scheme, namely: (i) using a L^2-projection Stokes solver à la Uzawa to force the incompressibility condition, (ii) an advection step, and (iii) a diffusion step. The resulting scheme reads as follows:

$$\mathbf{u}^0 = \mathbf{u}_0. \tag{5}$$

For $n \geq 0$, $\mathbf{u}^n \to \{\mathbf{u}^{n+1/3}, p^{n+1}\} \to \mathbf{u}^{n+2/3} \to \mathbf{u}^{n+1}$ via the solution of:

$$\begin{cases} \dfrac{\mathbf{u}^{n+1/3} - \mathbf{u}^n}{\Delta t} + \nabla p^{n+1} = \mathbf{0} \quad \text{in } \Omega, \\ \nabla \cdot \mathbf{u}^{n+1/3} = 0 \quad \text{in } \Omega, \\ \mathbf{u}^{n+1/3} \cdot \mathbf{n} = 0 \quad \text{on } \boldsymbol{\gamma}, \end{cases} \tag{6}$$

$$\begin{cases} \dfrac{\partial \mathbf{w}}{\partial t} + (\mathbf{u}^{n+1/3} \cdot \nabla)\mathbf{w} = \mathbf{0} \quad \text{in } \Omega \times (t^n, t^{n+1}), \\ \mathbf{w}(t^n) = \mathbf{u}^{n+1/3}, \\ \mathbf{w}(t) = \mathbf{u}_B(\mathbf{x}) \quad \text{on } \boldsymbol{\gamma}_-^{n+1} \times (t^n, t^{n+1}), \end{cases} \tag{7}$$

$$\mathbf{u}^{n+2/3} = \mathbf{w}(t^{n+1}), \tag{8}$$

$$\begin{cases} \dfrac{\mathbf{u}^{n+1} - \mathbf{u}^{n+2/3}}{\Delta t} - \mu \Delta \mathbf{u}^{n+1} = \mathbf{f}^{n+1} \quad \text{in } \Omega, \\ \mathbf{u}^{n+1} = \mathbf{u}_B(\mathbf{x}) \quad \text{on } \boldsymbol{\gamma}. \end{cases} \tag{9}$$

Two simplifications take place for the lid-driven cavity flow problem considered here: namely, $\mathbf{f} = \mathbf{0}$ and $\boldsymbol{\gamma}_-^{n+1} = \{\mathbf{x} | \mathbf{x} \in \boldsymbol{\gamma}, \mathbf{u}_B(\mathbf{x}) \cdot \mathbf{n}(\mathbf{x}) < 0\} = \emptyset$.

For the space discretization, we have used, as in [26, Chapter 5], [28], a P_1-iso-P_2 (resp., P_1) finite element approximation for the velocity field (resp., pressure) defined on uniform "tetrahedral" meshes $\mathcal{T}_h$ (resp., $\mathcal{T}_{2h}$). The three sub-problems in (6)–(9) are very classical problems

and each one of them can be solved by a variety of existing methods, this being one of the key points of the operator-splitting methodology. Sub-problem (6) (equivalent to a saddle-point problem) can be transformed into an elliptic problem for the pressure. But for the results presented in Section 3, it was solved by an Uzawa/preconditioned conjugate gradient algorithm as discussed in [26, Section 21]. Using the pressure obtained at the previous time step as the initial guess for the Uzawa algorithm, it takes one iteration except the first few hundred time steps. The advection problem (7)–(8) is solved by a wave-like equation method (see, e.g., [17, 18], [26, Section 31]) which is explicit and does not introduce numerical dissipation. Since the advection problem is decoupled from the others, a sub-time step satisfying the CFL condition can be chosen easily. The detailed scheme of wave-like equation method and properties can be found in, e.g., [18], [29, Chapter 3]. Sub-problem (9) is a classical elliptic problem which can be solved easily.

3. Numerical results

3.1. *Lid-driven flow in a cubic cavity*

For a lid-driven flow problem in a cubic cavity considered first in this section, we took $\Omega = (0,1)^3$ as computational domain and defined the Dirichlet data $\mathbf{u}_B$ by

$$\mathbf{u}_B(\mathbf{x}) = \begin{cases} (1,0,0)^T & \text{on } \{\mathbf{x} \mid \mathbf{x} = (x_1, x_2, 1)^T,\ 0 < x_1, x_2 < 1\}, \\ \mathbf{0} & \text{elsewhere on } \boldsymbol{\gamma}. \end{cases} \tag{10}$$

Then the Reynolds number is $Re = 1/\nu$. We assumed that a steady state has been reached when the change between two consecutive time steps, $\|\mathbf{u}_h^n - \mathbf{u}_h^{n-1}\|_\infty / \Delta t$, in the simulation is less than 10^{-7}, and then took $\mathbf{u}_h^n$ as the steady state solution.

To validate the numerical methodologies briefly described above, we have taken for the velocity mesh size the values $h = 1/80$, $1/120$, and $1/160$ associated with the time step $\Delta t = 0.001$. For $Re = 400$ and 1000, the results reported in Figure 2 show a very good agreement with those obtained in [30–32]. The steady flow velocity vectors for $Re = 400$ and 1000 are shown in Figure 3. Those velocity field vectors are projected onto the three planes, $x_2 = 0.5$, $x_1 = 0.5$, and $x_3 = 0.5$, and the length of the vectors has been enlarged two times in the two later planes to improve clarity. The plots show that the center of primary vortex moves down as Re increases from 400 to 1000 and secondary vortices appear in two lower corners, which is similar, in some sense, to what happens for the two-dimensional wall-driven cavity flow. At $x_1 = 0.5$, a pair of secondary vortices moves toward the lower corners as Re increases. Also another pair of vortices appears at the top corners. At $x_3 = 0.5$, there is a pair of secondary vortices near the upstream wall.

For $Re = 3200$ in a cubic cavity, experiments reported in [33] indicate that there are usually from two pairs of Taylor–Görtler-like (TGL) vortices. Moreover, these vortices are not stationary. Indeed, they meander to and from over the bottom wall closer to the downstream wall in the spanwise direction. In [34, 35], the number of pairs of TGL vortices obtained numerically varies between two and three. The results in Figure 4 obtained at $Re = 3200$ for $h = 1/120$ and $\Delta t = 0.001$ show that the time averaged speed profiles $u_1(0.5, 0.5, \cdot)$ and $u_3(\cdot, 0.5, 0.5)$ are in a good agreement with the experimental values obtained in [33]. Our simulation results show two to three pairs of TGL vortices at $Re = 3200$ as in Figure 5.

A well documented feature of three-dimensional lid-driven cavity flows is that they may exhibit Taylor–Görtler-like (TGL) vortices if Re is sufficiently large. Indeed, Iwatsu *et al.* [12] obtained a pairs of TGL vortices at $Re = 2000$. Also as predicted in [8, 9], a transition from steady flow to oscillatory one occurs at $Re_{\text{cr}} < 2000$. On the other hand, using a global linear stability analysis, Gianetti *et al.* found (Ref. [13]) that the cubic lid-driven cavity flow becomes

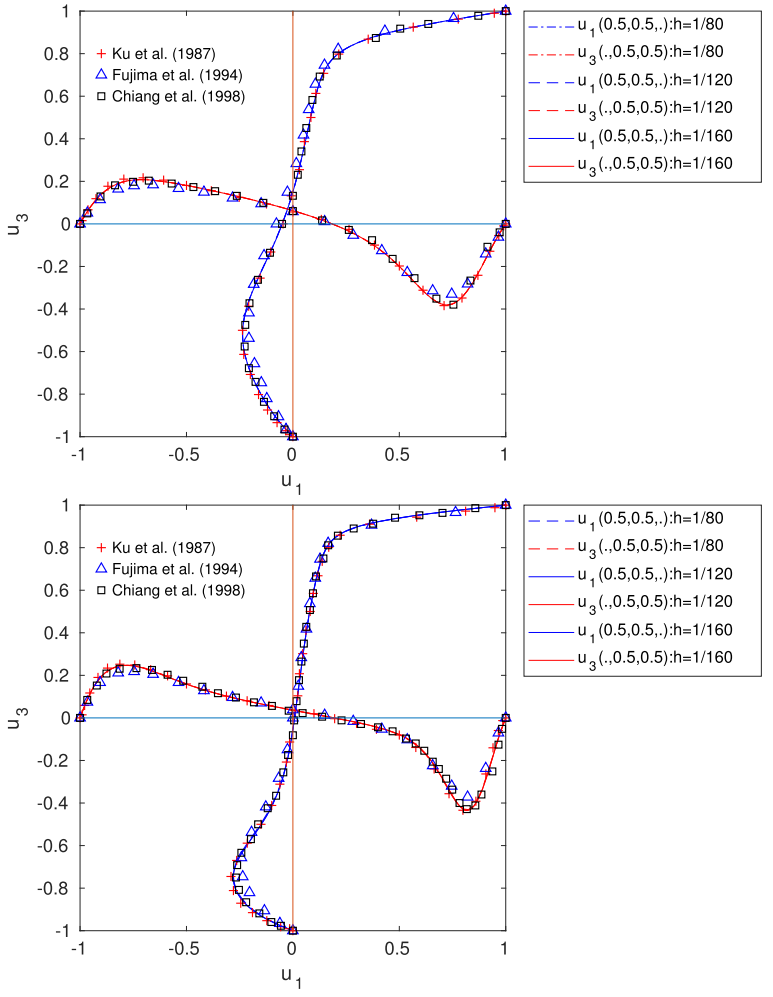

Figure 2. Comparisons of the numerical results obtained for $h = 1/80$, $1/120$, and $1/160$ at $Re = 400$ (top) and 1000 (bottom).

unstable for Re just above 2000. All these results indicate that the Hopf bifurcation is related to the existence of TGL vortices for Re slightly below 2000. Later, Kuhlmann and Albensoeder [11] also pinpointed that the critical Reynolds number value is 1919.51 and associated frequency is 0.58611.

We now want to locate the critical value of Reynolds number. As discussed above that if the Reynolds number value is increased beyond the critical value, the flow field in a cubic cavity switches to oscillatory one with the growth of oscillating amplitude in time. Thus, we have computed the flow velocity $\mathbf{u}_h^n$ for different values of Re and mesh size h and analyzed its history of L^2-norm (i.e., plot of $\|\mathbf{u}_h^n\|$ versus t). For $h = 1/120$, the flow field evolves to a steady state for $Re \le 1894$ and the amplitude of its L^2-norm oscillation decreases also in time. For $Re \ge 1895$, the steady state criterion is not satisfied and the amplitude of oscillation increases in time (see, Figure 6 for the case of $Re = 1900$). Thus we conclude that the critical Reynolds number $Re_{\rm cr}$ for the occurrence of transition is somewhere between 1894 and 1895. Applying the same analysis to the histories of flow velocity L^2-norm for $h = 1/160$ (see some of them in Figure 7), the critical

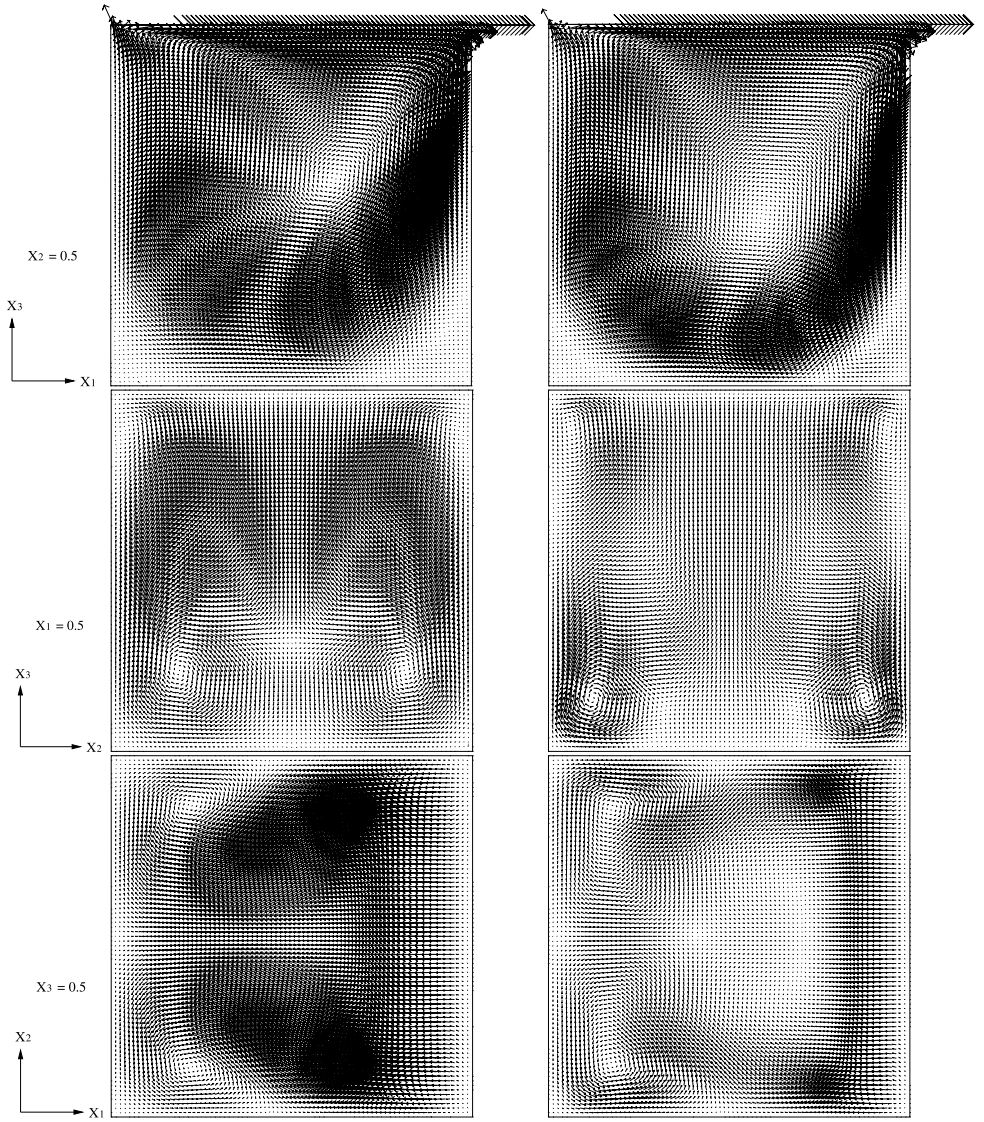

Figure 3. Steady flow velocity vector at $Re = 400$ (left) and 1000 (right) projected on the planes: $x_2 = 0.5$ (top), $x_1 = 0.5$ (middle), and $x_3 = 0.5$ (bottom) for $h = 1/160$ and $\Delta t = 0.001$. (In the middle and bottom plots, the vector scale is twice that of the actual one to enhance visibility.)

$Re_{\rm cr}$ is between 1913 and 1914. The oscillating frequency is between 0.5875 and 0.5860. These $Re_{\rm cr}$ and associated frequency for $h = 1/160$ are in a good agreement with obtained by Kuhlmann and Albensoeder in [11], which are 1919.51 and 0.58611, respectively.

3.2. *Lid-driven flow in shallow cavities*

To study the transition from steady flow to oscillating one in a shallow cavity with a unit square base, we have considered the lid-driven flow in a cavity $\Omega = [0,1] \times [0,1] \times [0,\Gamma]$ for $0 < \Gamma < 1$.

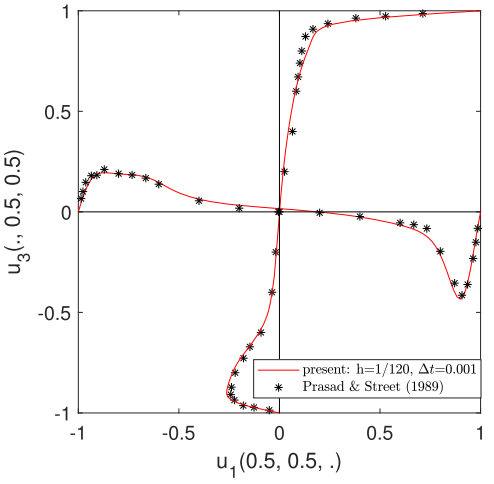

Figure 4. Comparisons of the time averaged numerical results obtained at $Re = 3200$ for $h = 1/120$ over 500 time units.

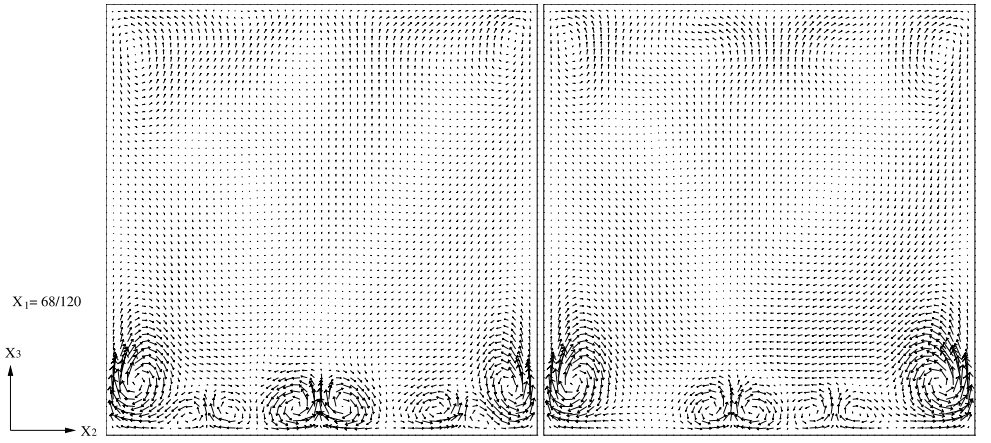

Figure 5. Projected velocity vectors on the plane $x_1 = 68/120$ at different instants of time showing interaction between TGL vortices and corner vortices at $Re = 3200$ for $h = 1/120$ and $\Delta t = 0.001$ (the vector scale is twice that of the actual one to enhance visibility).

The velocity mesh size is $h = 1/96$ and time step is $\Delta t = 0.001$. Following the approach used to obtain results presented in the previous section, we have located the critical Reynolds number for several values of height (Γ) as shown in Table 1. In [36], the linear-stability of steady two-dimensional lid-driven cavity flow in $\Omega = [0,\Gamma] \times [0,1]$ was studied. Their approach was actually considering the stability of such two-dimensional steady flow in a three-dimensional cavity with infinite depth. Unlike theirs, our study has taken into account the effect of all cavity boundary walls. Thus our results are different from theirs.

For those cavity heights presented in Table 1, we have studied how oscillating mode evolves when decreasing the height Γ via direct numerical simulation. For example, let us first study the case of $\Gamma = 3/4$ in details. The plots in Figure 8 show oscillations of the flow velocity L^2-norm, the oscillation amplitude being decreasing (resp., increasing) in time for $Re = 1721$ (resp., $Re = 1722$).

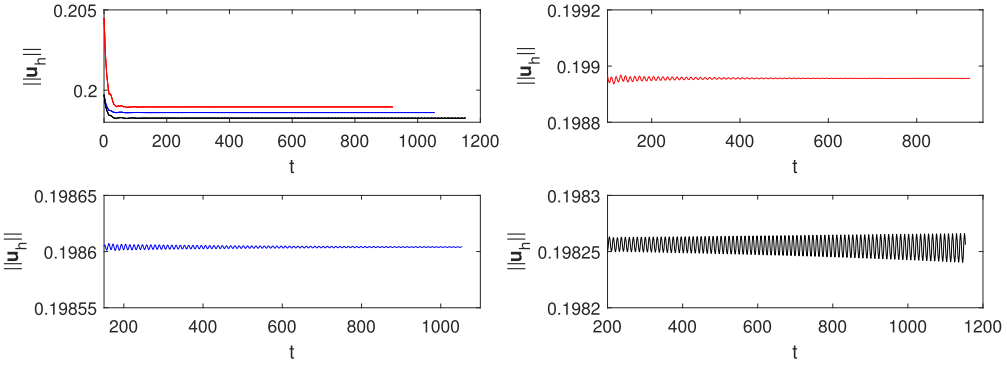

Figure 6. Histories of $\|\mathbf{u}_h\|$ for $Re = 1850$ (red), 1875 (blue), and 1900 (black) (top left plot) in a cubic cavity obtained with $h = 1/120$ and $\Delta t = 0.001$ and the enlargements for $Re = 1850$ (top right), 1875 (bottom left), and 1900 (bottom right).

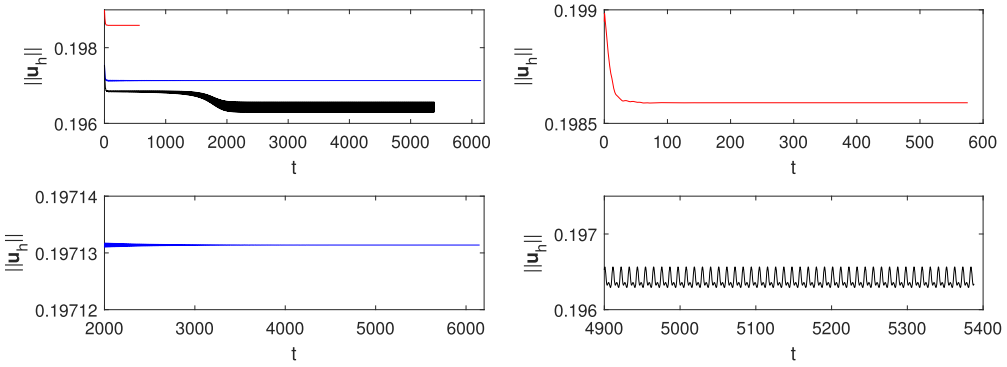

Figure 7. Histories of $\|\mathbf{u}_h\|$ for $Re = 1800$ (red), 1900 (blue), and 1920 (black) (top left plot) in a cubic cavity obtained with $h = 1/160$ and $\Delta t = 0.001$ and the enlargements for $Re = 1800$ (top right), 1900 (bottom left), and 1920 (bottom right).

Table 1. Critical Reynolds number is between Re_L (lower bound) and Re_U (upper bound) and associated frequencies are ω_L and ω_U. Those results are obtained with velocity mesh size $h = 1/96$ and time step $\Delta t = 0.001$

Γ	Re_L	Re_U	ω_L	ω_U
3/4	1721	1722	0.21974	0.21985
2/3	1656	1657	0.28777	0.28782
5/8	1689	1690	0.33755	0.33795
13/24	1730	1731	0.50557	0.50549
25/48	1522	1523	0.58394	0.58394
1/2	1364	1365	0.64127	0.64127
3/8	1179	1180	1.00114	1.00083

Thus its critical Reynolds number is between 1721 and 1722. To analyze the mode associated with those oscillations, we have selected one period of the oscillation for $Re = 1721$ and 1722,

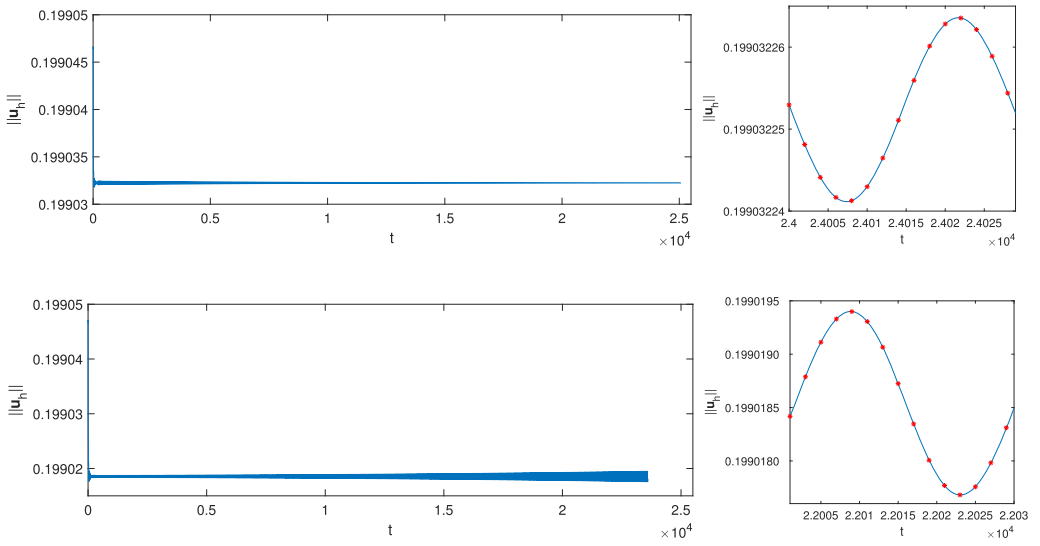

Figure 8. Histor of $\|\mathbf{u}_h\|$ (left) and that of one period (right) in a cavity of height $\Gamma = 3/4$ for $Re_L = 1721$ (top) and $Re_U = 1722$ (bottom). Each averaged velocity field is obtained by averaging those at the time marked by "*" shown in each plot.

respectively, as presented in Figure 8. The averaged velocity field of each Reynolds number is computed by averaging the velocity fields obtained at times marked by "*" in the right plots of Figure 8. The projections of averaged velocity field on the planes are shown in Figure 9, for both $Re = 1721$ and 1722, respectively. Although those projected velocity fields are almost identical to each other, we have plotted the difference between averaged velocity field and the one having about the maximum (resp. minimum) of $\|\mathbf{u}_h\|$ in Figures 10 and 11 for $Re = 1721$ and 1722, respectively. In Figure 10, the vector scale is either 25,000 or 10,000 times that of the actual one to enhance visibility due to the decreasing of oscillating amplitude in time for $Re = 1721$. But for $Re = 1722$ in Figure 11, the vector scale is either 2500 or 1000 times that of the actual one. When the values of $\|\mathbf{u}_h\|$ changes from the local maximum to local minimum (or vice versa), the vectors in Figures 10 and 11 change the direction to the opposite one. Obviously, the mode associated with the oscillation of $\|\mathbf{u}_h\|$ has been identified in Figures 10 and 11 for the cavity of height $\Gamma = 3/4$.

For $\Gamma = 2/3$, 5/8, 13/24, 25/48, 1/2, and 3/8, we have obtained similar flow results, but with some differences. In the following, flow field results obtained for $Re = Re_U$ are discussed due to the similarity of those obtained for $Re = Re_L$. In Figure 12, histories of $\|\mathbf{u}_h\|$ and selected one period are presented for $(\Gamma, Re) = (2/3, 1657)$, (5/8, 1690), (13/24, 1731), (25/48, 1523), (1/2, 1365), and (3/8, 1180). The associated averaged velocity fields projected on planes are shown in Figure 13. The size of main vortex becomes smaller when decreasing the value of Γ as shown in plots (a)–(f) in Figure 13. Similarly, two pairs of small vortices near the bottom of cavity are pushed toward lower corners and then disappeared when decreasing Γ from 3/4 to 3/8 (see Figure 9 and plots (g)–(l) in Figure 13). To show how the oscillating mode evolves for different values of the cavity height Γ, we have visualized the difference between averaged velocity field and the one having about the maximum value of $\|\mathbf{u}_h\|$ in Figure 14. When decreasing Γ value from 3/4 to 2/3, the number of vortices near the bottom of cavity increases. Then the middle vortices become weaker when Γ goes from 2/3 to 13/24. When changing

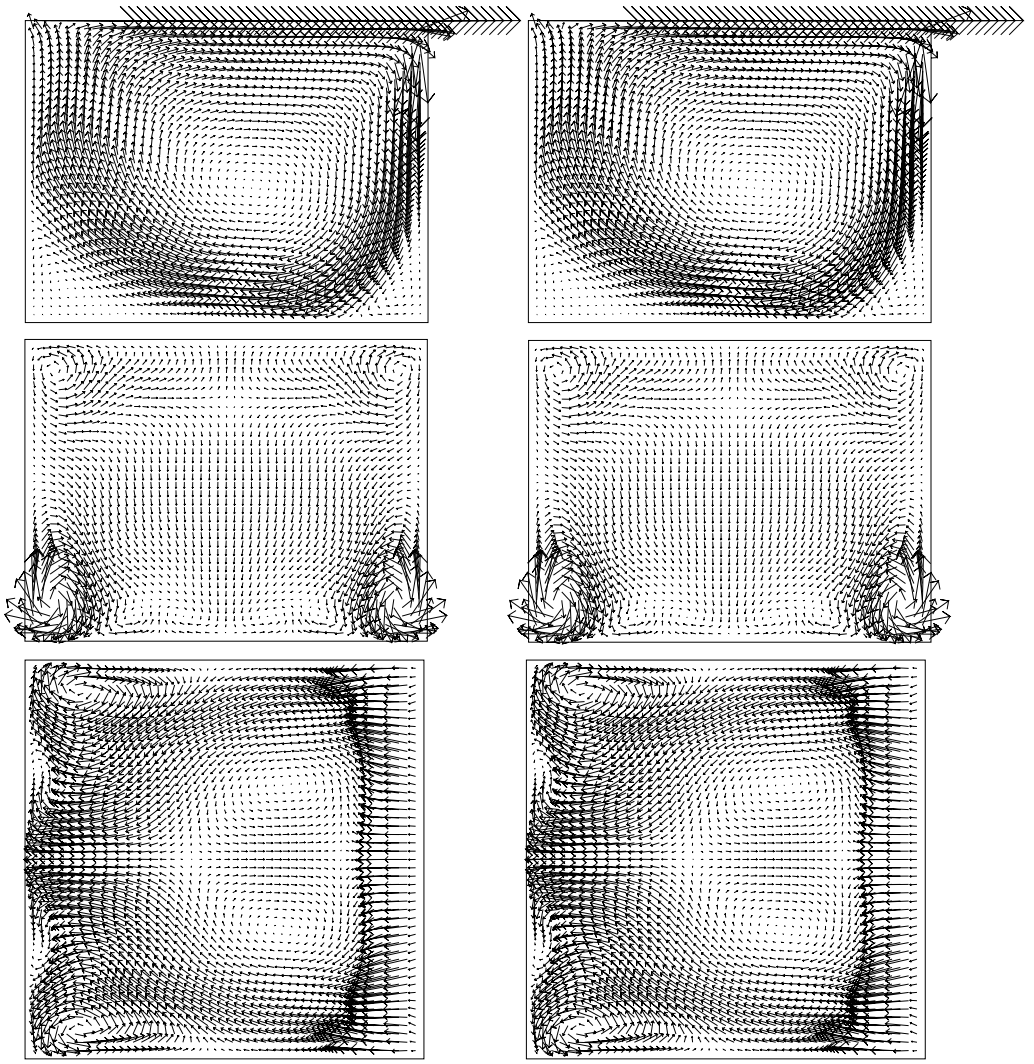

Figure 9. Projected averaged flow velocity vector on the planes: $x_2 = 0.5$ (top), $x_1 = 0.625$ (middle), and $x_3 = 0.375$ (bottom) in a cavity of height $\Gamma = 3/4$: (i) $Re_L = 1721$ for $24{,}000 \le t \le 24{,}028.596$ (left three) and (ii) $Re_U = 1722$ for $22{,}001 \le t \le 22{,}029.58$ (right three). (In the middle and bottom plots, the vector scale is four times that of the actual one to enhance visibility.)

Γ from 13/24 to 1/2, the middle vortices next to the bottom wall disappear. Also the major one next to the top wall is gone. Finally for Γ changing from 1/2 to 3/8, four new vortices are observed in the middle region. The disappearance of those middle vortices is quite unusual. We believe that this change of the oscillating mode is one of the reasons why the critical Reynolds numbers suddenly become smaller for $\Gamma = 1/2$, and 3/8 as in Table 1. For the study of two-dimensional lid-driven flow in shallow cavities obtained in [36], the critical Reynolds number increases when decreasing Γ to zero. Our result of the critical Reynolds number is different since their cavity has infinite depth (i.e., there are no walls in the depth direction).

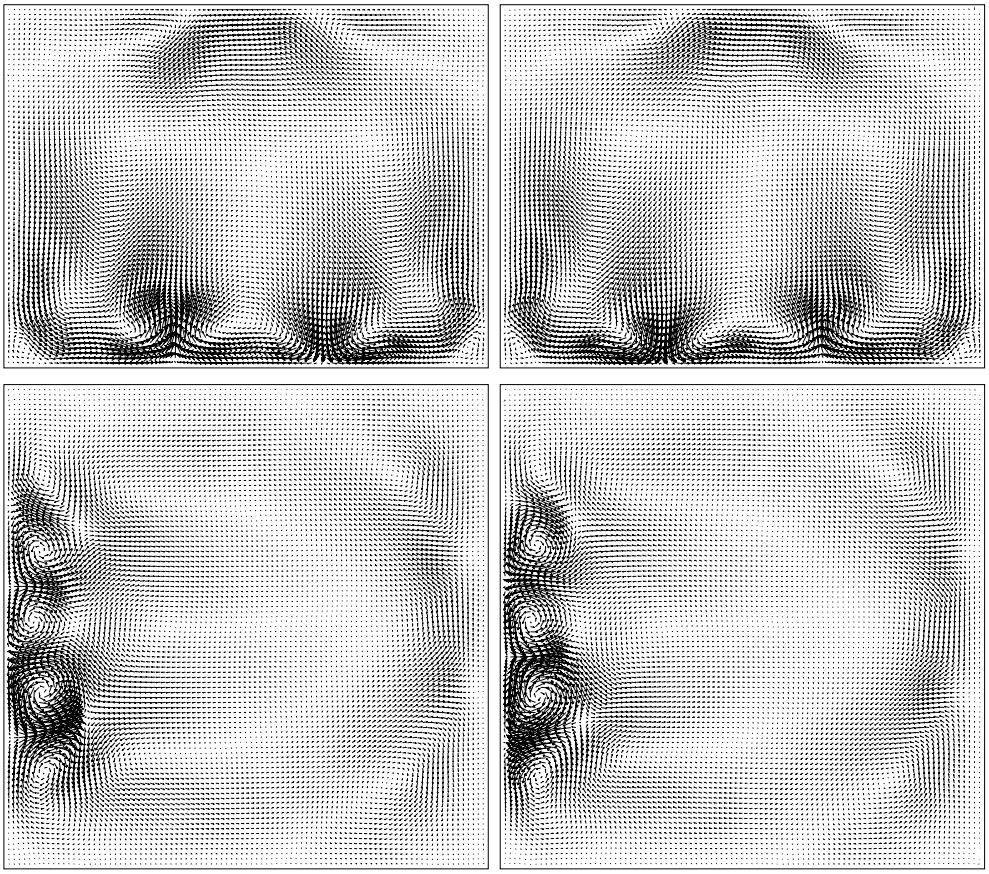

Figure 10. Projected velocity field of the difference between the averaged velocity field and the ones at $t = 24{,}008$ (left) and $t = 24{,}022$ (right), respectively, on the planes $x_1 = 0.625$ (top) and $x_3 = 0.375$ (bottom) for $Re_L = 1721$ in a cavity of height $\Gamma = 3/4$ where the minimum (resp., maximum) of $\|\mathbf{u}_h\|$ occurs at about $t = 24{,}008$ (resp., $t = 24{,}022$) for $24{,}000 \le t \le 24{,}028.596$ as in Figure 8. (In the upper (resp., lower) two plots, the vector scale is 25000 (resp., 10,000) times that of the actual one to enhance visibility.)

4. Conclusion

In this article, we have studied numerically the transition from steady flow to oscillatory one in cavities via a three-stage Lie's scheme. The numerical results obtained for $Re = 400$, 1000 and 3200 in a cubic cavity show a good agreement with numerical and experimental results available in the literature. Our simulation results show that the value of critical Reynolds number $Re_{\rm cr}$ for for having flow with increasing of oscillating amplitude (a Hopf bifurcation) lie somewhere in the interval (1913, 1914) for $h = 1/160$. The oscillating frequency is between 0.5875 and 0.5860. The $Re_{\rm cr}$ and associated frequency for $h = 1/160$ are in a good agreement with obtained by Kuhlmann and Albensoeder in [11]. Then the flow velocity distortion at Re close to $Re_{\rm cr}$ in shallow cavities has been investigated. We have visualized the how oscillating mode evolves for different values of the cavity height Γ. When decreasing Γ value from 3/4 to 2/3, the number of vortices near the bottom of cavity increases. Then the middle vortices close to the bottom wall become weaker when Γ goes from 2/3 to 25/48. But for $\Gamma = 1/2$ and 3/8, the disappearance of those middle vortices occurs.

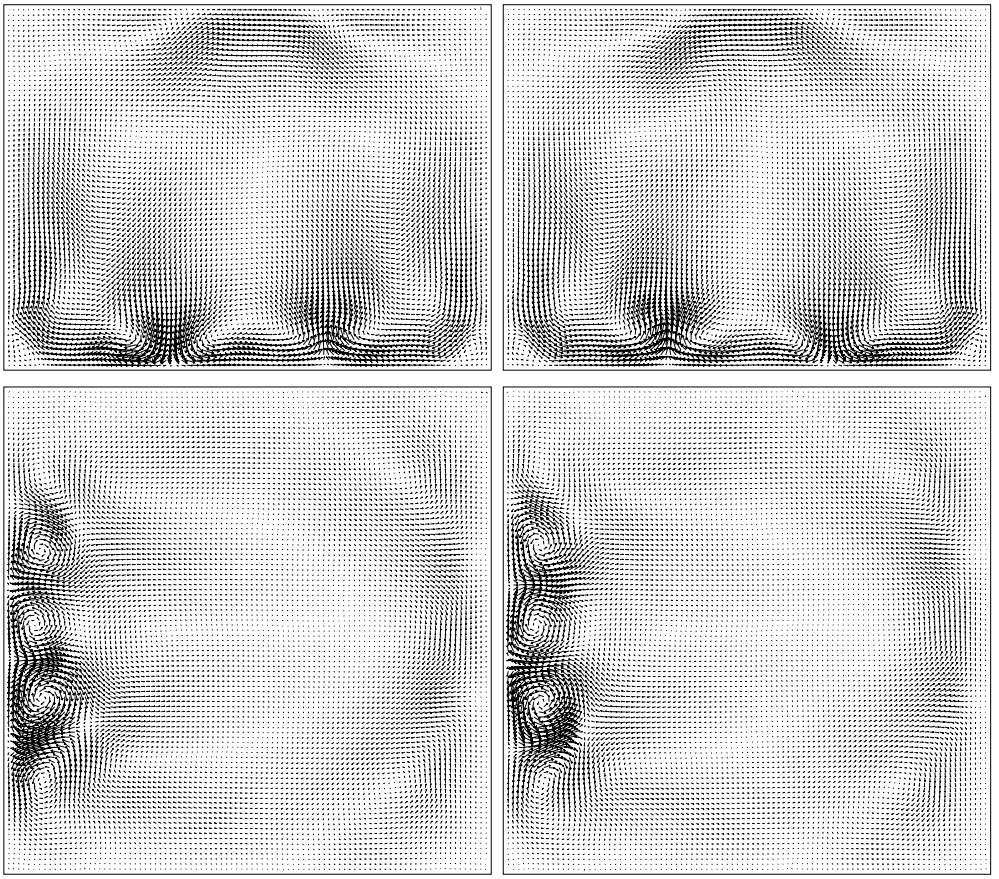

Figure 11. Projected velocity field of the difference between the averaged velocity field and the ones at $t = 22{,}009$ (left) and $t = 22{,}023$ (right), respectively, on the planes $x_1 = 0.625$ (top) and $x_3 = 0.375$ (bottom) for $Re_U = 1722$ in a cavity of height $\Gamma = 3/4$ where the maximum (resp., minimum) of $\|\mathbf{u}_h\|$ occurs at about $t = 22{,}009$ (resp., $t = 22{,}023$) for $22{,}001 \le t \le 22{,}029.58$ as in Figure 8. (In the upper (resp., lower) two plots, the vector scale is 2500 (resp., 1000) times that of the actual one to enhance visibility.)

We believe that this change of the oscillating mode is one of the reasons why critical Reynolds numbers suddenly becomes smaller for $\Gamma = 1/2$ and $3/8$. Our results are different from those obtained by the linear stability study of two-dimensional flow.

Conflicts of interest

The authors declare no competing financial interest.

Dedication

The manuscript was written through contributions of all authors. All authors have given approval to the final version of the manuscript.

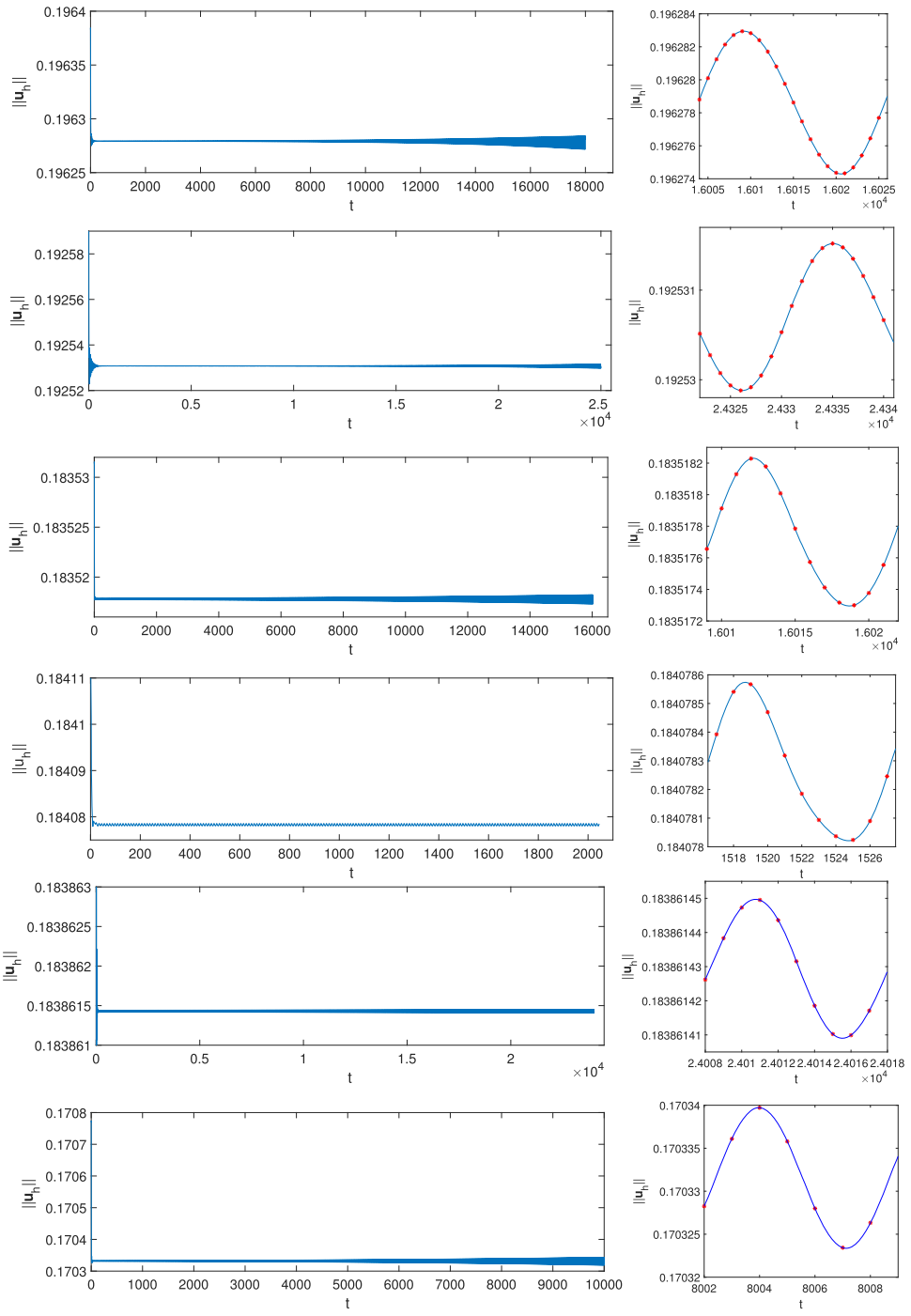

Figure 12. History of $\|\mathbf{u}_h\|$ (left) and that of one period (right) in a cavity for (Γ, Re_U) = (2/3, 1657), (5/8, 1690), (13/24, 1731), (25/48, 1523), (1/2, 1365), and (3/8, 1180) (from top to bottom). Each averaged velocity field is obtained by averaging those at times marked by "*".

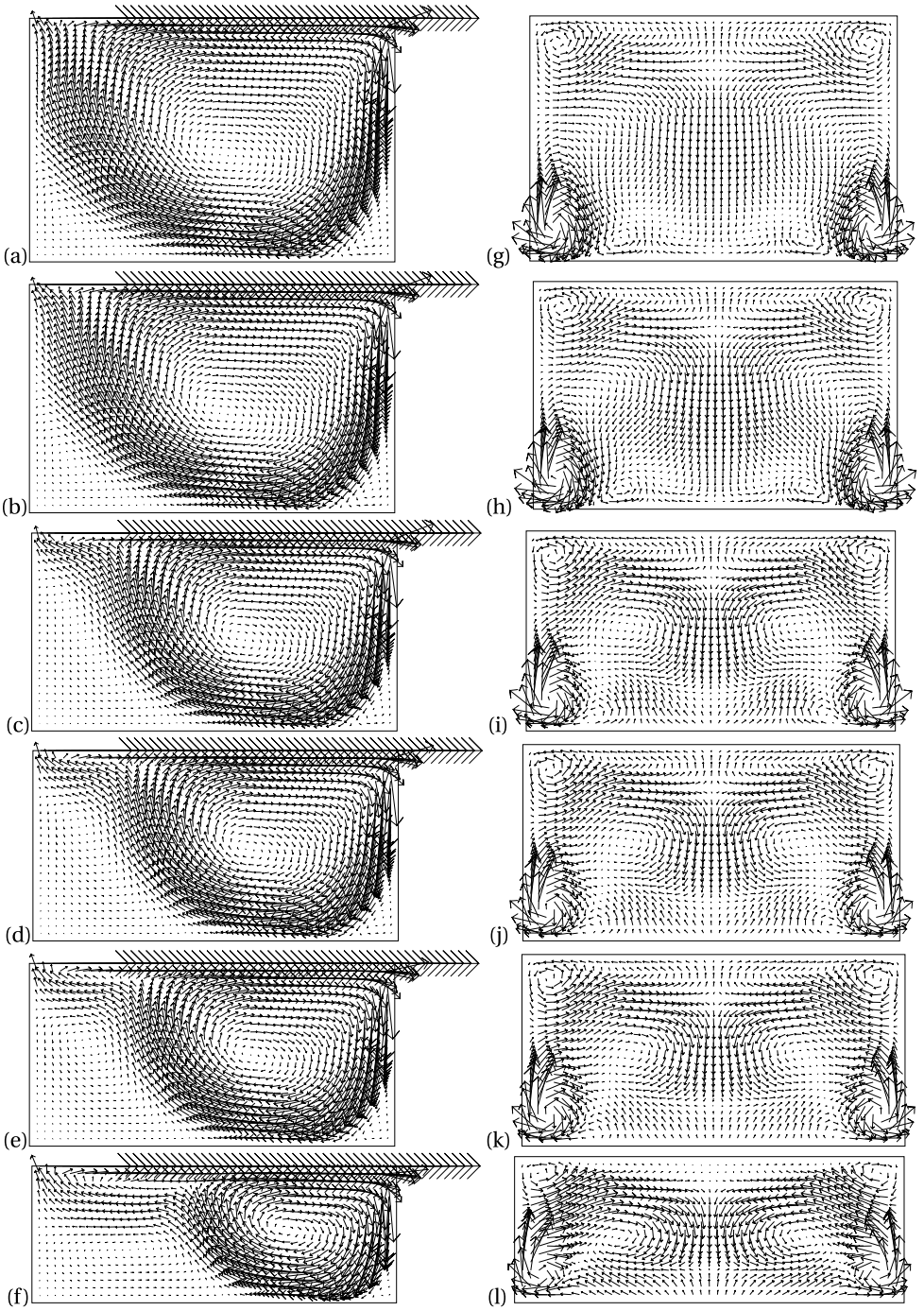

Figure 13. Projected averaged flow velocity vector on the planes: (a)–(f) $x_2 = 0.5$, (g) $x_1 = 62/96$, (h) $x_1 = 64/96$, (i) $x_1 = 65/96$, (j) $x_1 = 66/96$, (k) $x_1 = 67/96$, and (l) $x_1 = 73/96$ for $(\Gamma, Re_U) = (2/3, 1657)$, $(5/8, 1690)$, $(13/24, 1731)$, $(25/48, 1523)$, $(1/2, 1365)$, and $(3/8, 1180)$ (from top to bottom). (In plots (g)–(l) the vector scale is four times that of the actual one to enhance visibility comparing those in plots (a)–(f).)

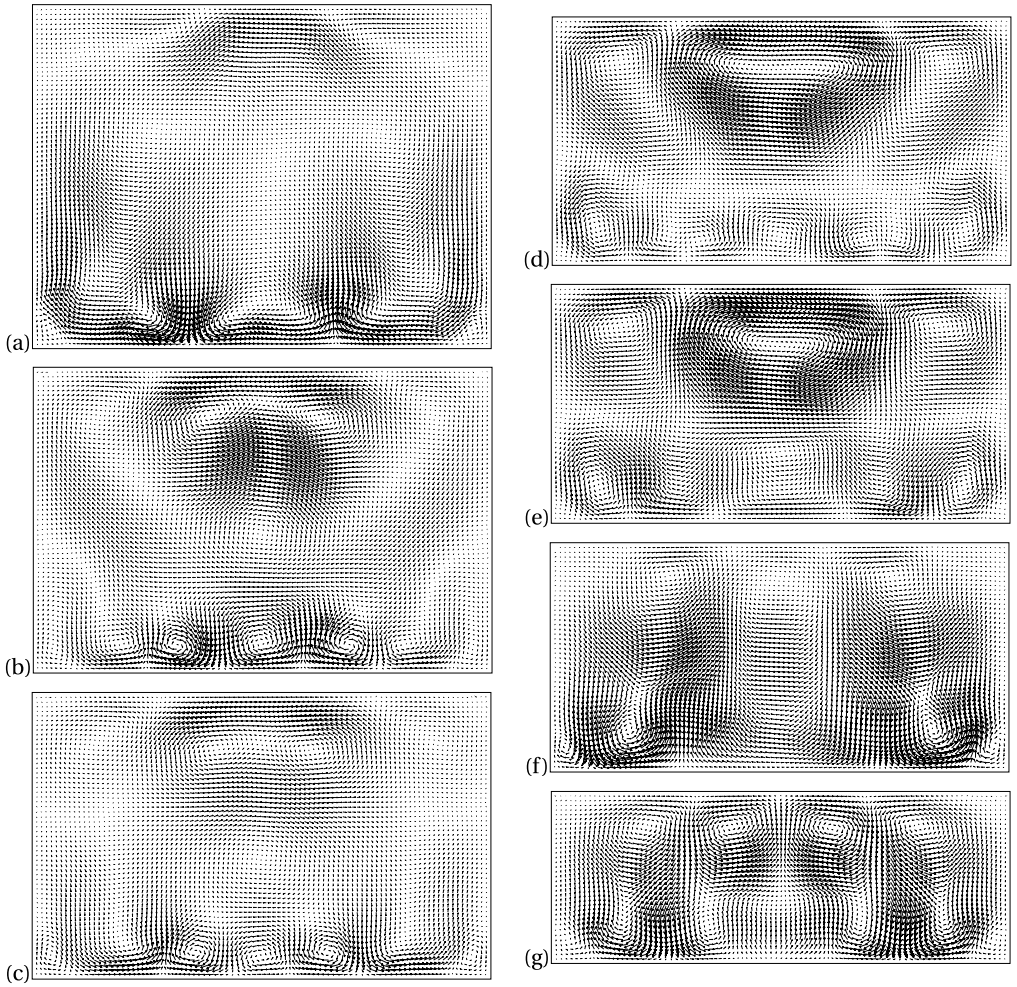

Figure 14. Projected velocity field of the difference between averaged velocity field and the one having about the maximum value of $\|\mathbf{u}_h\|$: (a) $x_1 = 60/96$, (b) $x_1 = 62/96$, (c) $x_1 = 64/96$, (d) $x_1 = 65/96$, (e) $x_1 = 66/96$, (f) $x_1 = 67/96$, and (g) $x_1 = 73/96$ for $(\Gamma, Re_U) = (3/4, 1722)$, (2/3, 1657), (5/8, 1690), (13/24, 1731), (25/48, 1523), (1/2, 1365), and (3/8, 1180) (from top to bottom and from left to right). (All the vector fields are magnified.)

Acknowledgments

Lid-driven cavity flow problem was one of Professor Roland Glowinski's favorite research topics. The first version of this article was done with Roland several years ago. But due to some technical issues, it was not published. We started revising it with Roland a year ago. Sadly this revised article was not ready till now.

References

[1] C. K. Aidun, N. G. Triantafillopoulos, J. D. Benson, "Global stability of a lid-driven cavity with throughflow: Flow visualization studies", *Phys. Fluids A* **3** (1991), p. 2081-2091.

[2] P. N. Shankar, M. D. Deshpande, "Fluid mechanics in the driven cavity", *Annu. Rev. Fluid Mech.* **32** (2000), p. 93-136.

[3] O. Goyon, "High-Reynolds number solutions of Navier–Stokes equations using incremental unknowns", *Comput. Methods Appl. Mech. Eng.* **130** (1996), p. 319-335.
[4] F. Auteri, N. Parolini, L. Quartapelle, "Numerical investigation on the stability of singular driven cavity flow", *J. Comput. Phys.* **183** (2002), p. 1-25.
[5] M. Sahin, R. G. Owens, "A novel fully implicit finite volume method applied to the lid-driven cavity problem. Part II: Linear stability analysis", *Int. J. Numer. Meth. Fluids* **42** (2003), p. 79-88.
[6] C. H. Bruneau, M. Saad, "The 2D lid-driven cavity problem revisited", *Comput. Fluids* **35** (2006), p. 326-348.
[7] T. Wang, T.-W. Pan, R. Glowinski, "A comparison of L^2-projection and H^1-projection methods for the numerical simulation of incompressible viscous fluid flow: A case study", *Chin. J. Eng. Math.* **25** (2008), p. 761-778.
[8] Y. Feldman, A. Y. Gelfgat, "Oscillatory instability of a three-dimensional lid-driven flow in a cube", *Phys. Fluids* **22** (2010), article no. 093602.
[9] A. Liberzon, Y. Feldman, A. Y. Gelfgat, "Experimental observation of the steady-oscillatory transition in a cubic lid-driven cavity", *Phys. Fluids* **23** (2011), article no. 084106.
[10] K. Anupindi, W. Lai, S. Frankel, "Characterization of oscillatory instability in lid driven cavity flows using lattice Boltzmann method", *Comput. Fluids* **92** (2014), p. 7-21.
[11] H. C. Kuhlmann, S. Albensoeder, "Stability of the steady three-dimensional lid-driven flow in a cube ans the supercritical flow dynamics", *Phys. Fluids* **26** (2014), article no. 024104.
[12] R. Iwatsu, J. M. Hyun, K. Kuwahara, "Analyses of three-dimensional flow calculations in a driven cavity", *Fluid Dyn. Res.* **6** (1990), p. 91-102.
[13] F. Giannetti, P. Luchini, L. Marino, "Linear stability analysis of three-dimensional lid-driven cavity flow", in *Atti del XIX Congresso AIMETA di Meccanica Teorica e Applicata*, Aras Edizioni Ancona, Italy, 2009.
[14] A. J. Chorin, T. J. R. Hughes, M. F. McCracken, J. E. Marsden, "Product formulas and numerical algorithms", *Commun. Pure Appl. Math.* **31** (1978), p. 205-256.
[15] R. Glowinski, G. Guidoboni, T.-W. Pan, "Wall-driven incompressible viscous flow in a two-dimensional semi-circular cavity", *J. Comput. Phys.* **216** (2006), p. 79-91.
[16] T.-W. Pan, R. Glowinski, "A projection/wave-like equation method for the numerical simulation of incompressible viscous fluid flow modeled by the Navier–Stokes equations", *Comput. Fluid Dyn. J.* **9** (2009), p. 28-42.
[17] E. J. Dean, R. Glowinski, "A wave equation approach to the numerical solution of the Navier–Stokes equations for incompressible viscous flow", *C. R. Acad. Sci. Paris Sér. I* **325** (1997), p. 783-791.
[18] J. Hao, T.-W. Pan, R. Glowinski, D. D. Joseph, "A fictitious domain/distributed Lagrange multiplier method for the particulate flow of Oldroyd-B fluids: A positive definiteness preserving approach", *J. Non-Newtonian Fluid Mech.* **156** (2009), p. 95-111.
[19] A. J. Chorin, "A numerical method for solving incompressible viscous flow problems", *J. Comput. Phys.* **2** (1967), p. 12-26.
[20] A. J. Chorin, "Numerical solution of the Navier–Stokes equations", *Math. Comput.* **23** (1968), p. 341-354.
[21] R. Temam, "Sur l'approximation des équations de Navier–Stokes par la méthode des pas fractionnaires (I)", *Arch. Rat. Mech. Anal.* **32** (1969), p. 135-153.
[22] R. Temam, "Sur l'approximation des équations de Navier–Stokes par la méthode des pas fractionnaires (II)", *Arch. Rat. Mech. Anal.* **33** (1969), p. 377-385.
[23] G. I. Marchuk, "Splitting and alternating direction methods", in *Handbook of Numerical Analysis* (P. G. Ciarlet, J.-L. Lions, eds.), vol. I, North-Holland, Amsterdam, 1990.
[24] S. Turek, "A comparative study of time-stepping techniques for the incompressible Navier–Stokes equations: from fully implicit nonlinear schemes to semi-implicit projection methods", *Int. J. Numer. Math. Fluids* **22** (1996), p. 987-1011.
[25] M. Marion, R. Temam, "Navier–Stokes equations", in *Handbook of Numerical Analysis* (P. G. Ciarlet, J.-L. Lions, eds.), vol. VI, North-Holland, Amsterdam, 1998.
[26] R. Glowinski, "Finite element methods for incompressible viscous flow", in *Handbook of Numerical Analysis* (P. G. Ciarlet, J.-L. Lions, eds.), vol. IX, North-Holland, Amsterdam, 2003.
[27] R. Glowinski, S. J. Osher, W. Yin (eds.), *Splitting Methods in Communication, Imaging, Science, and Engineering*, Springer, Cham, Switzerland, 2017.
[28] M. O. Bristeau, R. Glowinski, J. Périaux, "Numerical methods for the Navier–Stokes equations. Applications to the simulation of compressible and incompressible viscous flow", *Comput. Phys. Rep.* **6** (1987), p. 73-187.
[29] R. Glowinski, T.-W. Pan, *Numerical Simulation of Incompressible Viscous Flow: Methods and Applications*, De Gruyter, Berlin/Boston, 2022.
[30] S. Fujima, M. Tabata, Y. Fukasawa, "Extension to three-dimensional problems of the upwind finite element scheme based on the choice up- and downwind points", *Comput. Meth. Appl. Mech. Eng.* **112** (1994), p. 109-131.
[31] H. C. Ku, R. S. Hirsh, T. D. Taylor, "A pseudospectral method for solution of the three-dimensional incompressible Navier–Stokes equations", *J. Comput. Phys.* **70** (1987), p. 439-462.

[32] T. P. Chiang, W. H. Sheu, R. R. Hwang, "Effect of Reynolds number on the eddy structure in a lid-driven cavity", *Int. J. Numer. Methods Fluids* **26** (1998), p. 557-579.
[33] A. K. Prasad, J. R. Koseff, "Reynolds number and end-wall effects on a lid-driven cavity flow", *Phys. Fluids A: Fluid Dyn.* **1** (1989), p. 208-218.
[34] C. Y. Perng, R. L. Street, "Three-dimensional unsteady flow simulations: Alternative strategies for a volume-averaged calculation", *Int. J. Numer. Math. Fluids* **9** (1989), p. 341-362.
[35] C. M. Teixeira, "Digital physics simulation of lid-driven cavity flow", *Int. J. Mod. Phys. C* **8** (1997), p. 685-696.
[36] S. Albensoeder, H. C. Kuhlmann, H. J. Rath, "Three-dimensional centifugal-flow instabilities in a lid-driven-cavity problem", *Phys. Fluids* **13** (2001), p. 121-135.